Relaxation dynamics in laser-excited metals under nonequilibrium conditions

B. Y. Mueller* and B. Rethfeld

Department of Physics and Research Center OPTIMAS, University of Kaiserslautern, Erwin-Schrödinger-Str. 46, 67663 Kaiserslautern, Germany

(Received 19 October 2012; revised manuscript received 21 December 2012; published 30 January 2013)

When an ultrashort laser pulse irradiates a metal, energy is absorbed by the electron system which is driven out of thermal equilibrium on a femtosecond time scale. Due to electron-electron collisions, a new thermodynamical equilibrium state within the electron system is established in a characteristic time, the so-called thermalization time. The absorbed energy of the electrons will be further transferred to the phononic system. The thermalization time as well as the electron-phonon coupling strength both strongly depend on the material properties and the excitation type. Furthermore, a nonthermalized electron gas couples differently to the phononic system as a thermalized one. In order to follow the relevant microscopic dynamics without the need to assume thermalized electrons, we apply complete Boltzmann collision integrals to describe the transient electron distribution due to excitation, thermalization, and relaxation. We implement the density of states of real materials in our approach. As a result of our simulations, we extract the electron thermalization time and the electron-phonon coupling under nonequilibrium conditions. Examples are given for aluminum, gold, and nickel.

DOI: 10.1103/PhysRevB.87.035139 PACS number(s): 71.20.−b, 79.20.Ap, 71.38.−k, 05.70.Ln

I. INTRODUCTION

Ultrashort laser pulses of moderate intensities are widely applied in basic research as well as in medical and industrial applications.[1–3] Ultrafast excitations of solids open up opportunities to study microscopic processes on femtosecond time scales as electron-electron interaction or electron-phonon coupling. Such processes and their interplay have been the object of intense research for more than two decades both experimentally and theoretically.[4–21] Several theoretical approaches investigating the response of solids on ultrashort laser excitation are currently applied on a wide range of time scales. They reach from temperature-dependent density functional theory (DFT) methods yielding changes of the band structure upon excitation,[22–24] statistical approaches tracing a large amount of excited electrons,[15–19] over two-temperature descriptions and continuum approaches of heat conduction[12,25,26] to hydrodynamic and molecular dynamic descriptions[7,27–31] of the subsequent phase transitions and material removal. In this work, we focus on the subpicosecond time scale, where energy relaxation processes of the electronic system are most relevant. The governing collision processes occur on femtosecond time scale, thus appropriate descriptions have to be chosen carefully. Typically, the absorption of the laser by the electron system and the energy transfer to the initially cold lattice is described by the well-known two-temperature model (TTM) for the electron temperature T_e and the phonon temperature T_p (Ref. 32):

$$\begin{aligned} C_e(T_e)\frac{\partial T_e}{\partial t} &= -\alpha(T_e - T_p) + \nabla(\varkappa_e \nabla T_e) + S(t), \\ C_p(T_p)\frac{\partial T_p}{\partial t} &= +\alpha(T_e - T_p), \end{aligned} \tag{1}$$

where C_e,C_p are the heat capacities of the electrons and phonons, $S(t)$ the excitation term, α the electron-phonon coupling factor, and $\varkappa_e$ the heat conductivity. The TTM is suitable to describe laser-excited metals on time scales of a few hundreds of femtoseconds to tens of picoseconds.[9–11,33,34] It is widely applied in the description of material processing as, for instance, hole drilling[35] or ripple formation.[21,36] Several extensions have been proposed to account also for ballistic transport,[10] field emission,[37] nonthermal electrons,[12,38] as well as changes in the density of the solid.[25] The necessary material parameters for a large variety of metals have been determined on the basis of the respective densities of states calculated with DFT methods.[39] The TTM was applied as well to describe ultrafast magnetization dynamics[40,41] or energy dissipation after excitation with a swift heavy ion.[42,43]

However, on time scales below a few hundreds of femtoseconds, the nonequilibrium of the electrons may come into play. The electrons, driven out of thermodynamic equilibrium by ultrafast excitation mechanisms, thermalize on these time scales, establishing a new equilibrium state by electron-electron collisions. Before completion of this process, the concept of temperature, strictly spoken, fails, and therefore the application of the TTM is questionable in the first hundreds of femtoseconds after excitation.

The Boltzmann equation[13–17] or Monte Carlo methods[18,19] are suitable models to trace the nonequilibrium electrons and to study thermalization dynamics and electron-phonon coupling in detail. Consequently, an interesting question arises: Under which conditions do the assumptions of the TTM hold and in which cases are more accurate models required? To answer this question, we apply the framework of the Boltzmann equation to describe metals under nonequilibrium conditions. We derive complete Boltzmann collision integrals including arbitrary densities of states within an effective one-band model. We are first interested in the thermalization time of the electron system. This characteristic time determines when the concept of a temperature can be applied and depends on the material as well as on the excitation. In addition, we extract the electron-phonon coupling parameter α which is used within the TTM (1). We compare the equilibrium coupling, where T_e and T_p are well defined, with the nonequilibrium energy exchange when electrons are out of thermal equilibrium. The calculations presented in this work are performed for three different materials: aluminum, gold, and nickel. However, in

 ©2013 American Physical Society

principle, all metals can be implemented in the presented framework if some fundamental material parameters as well as the density of states are known.

II. BOLTZMANN EQUATION FOR METALS

We apply the Boltzmann equation for the description of nonequilibrium effects. This approach is suitable to model collisions of particles such as electrons and phonons and was originally derived for plasma physics but also successfully applied for solids.[13–17,44–49] We restrict ourselves to thin films which are excited homogeneously by a laser pulse (the effective penetration depth of the laser is assumed to be much larger than the thickness of the film), so no heat transfer is considered. For example, for gold films the effective penetration depth of homogeneous heating is about 100 nm.[50]

Therefore, the Boltzmann equation without a spatial dependence is applied, which reads as

$$\frac{df(\vec{k},t)}{dt} = \Gamma_{\text{el-el}} + \Gamma_{\text{el-ph}} + \Gamma_{\text{absorp}}, \tag{2a}$$

$$\frac{dg(\vec{q},t)}{dt} = \Gamma_{\text{ph-el}}, \tag{2b}$$

where $f(\vec{k},t)$ is the distribution of the electrons with momentum $\vec{k}$ and $g(\vec{q},t)$ the distribution of the phonons with momentum $\vec{q}$. The complete Boltzmann collision integrals Γ_{x-y} describe collisions of particles x with particles y and Γ_{absorp} denotes the collision integral due to the excitation of the electrons by inverse bremsstrahlung.[17] Typically, the set of equations (2) is simplified by applying a free-electron-gas approach[13,16,17,45] and by the assumption of isotropy, i.e., the distribution functions $f(\vec{k},t)$, $g(\vec{q},t)$ only depend on the absolute value of the momentum and, thus, are rewritten to an dependence on energy $f(E,t)$ and $g(E_q,t)$.

In the following, we still keep the isotropy of the system but show the extension for more realistic cases, including a realistic density of states (DOS) in the frame of an effective one-band model. A similar approach has also been proposed in Ref. 15 implementing the DOS into the Boltzmann equation, however, considering a constant matrix element. Here, we treat the matrix element explicitly by a screened Coulomb potential and, moreover, include transient changes of the screening parameter under nonequilibrium conditions.

Instead of the complete band structure of the material, we introduce an effective one-band model, where an averaged isotropic dispersion relation is derived out of the density of states. Specific band-structure effects are thus only treated by the averaged band and by the density of states. This simplification is justified for electron-electron as well as electron-phonon collisions since both electrons and phonons provide sufficient momentum to conserve the energy and momentum during a scattering process in the framework of the isotropic approximation. The irradiation process has to be modeled more carefully since photons provide a relative small momentum. We therefore implement an absorption term of inverse bremsstrahlung, which accounts for the potential of the lattice ions providing momentum changes to the quasifree electrons.[17]

Let us first consider an arbitrary isotropic extensive observable $B(E)$ of the electron or phonon system which is examined by introducing the density of states $D(E)$:

$$\langle B\rangle = \frac{\sigma}{(2\pi)^3}\int d\vec{r}\int d\vec{k}\; h(E)\cdot B(E) \tag{3a}$$

$$\equiv \Omega\int dE\; D(E)\cdot h(E)\cdot B(E), \tag{3b}$$

where $\Omega \equiv \int d\vec{r}$ represents the volume of the unit cell and $h(E)$ the isotropic distribution function of the considered particles, i.e., $f(E)$ or $g(E)$. In our notation, σ determines the spin factor which is two for the electron system and one for the phonons. From Eq. (3), we extract the definition of the density of states

$$D(E) = \frac{\sigma}{2\pi^2}k^2(E)\frac{dk}{dE}, \tag{4}$$

which only depends on the dispersion relation $k(E)$. In the effective one-band model, we solve the differential equation (4) analytically for the momentum

$$k(E) = \sqrt[3]{\frac{3\cdot 2\pi^2}{\sigma}\int_0^E d\epsilon\; D(\epsilon)}, \tag{5}$$

which results in an averaged isotropic dispersion relation to determine the momentum k corresponding to the energy E. To give an example, by inserting a free-electron-gas density of states, we obtain the dispersion relation of free electrons $k = \sqrt{2mE/\hbar^2}$ with the effective electron mass m. In Fig. 1, the density of states of nickel[39] and the corresponding one-band dispersion relation is depicted. Despite the roughness of the DOS, the integral in Eq. (5) smooths the behavior of $k(E)$. Furthermore, the flatness of the d bands is reflected in the averaged dispersion relation. Basically, we assume one band with an energy-dependent effective mass, derived by the density of states. Since we treat the material as isotropic, the dispersion and the observables are isotropic as well. Our approach allows us to account for specific effects caused

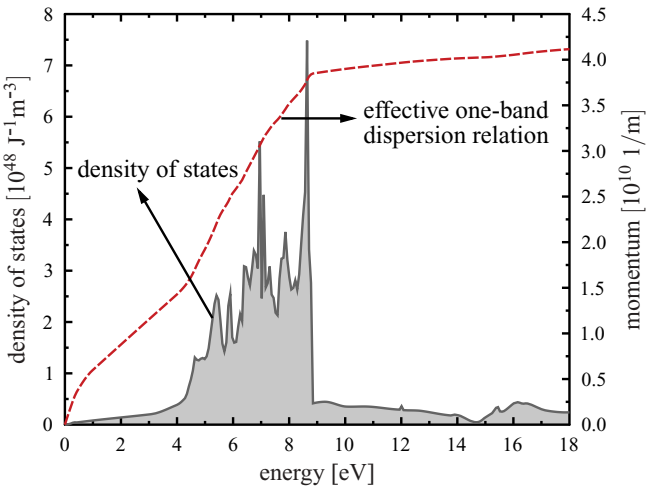

FIG. 1. (Color online) The density of states of nickel (left axis) and the corresponding averaged dispersion relation (right axis) in the framework of the effective one-band model.

by distinct peaks or gaps in the density of states, while effects connected with the particular band structure, e.g. state blocking,[51] are neglected. In agreement with temperature-dependent DFT calculations,[22–24,52] we assume that the DOS after the laser irradiation is qualitatively unaffected for our considered excitation strength.

A. Electron-electron collisions

To derive the electron-electron collision integral, we consider two electrons with the total initial energy $E_i = E + E_2$ and the final energy $E_f = E_1 + E_3$ after the collision. During the scattering process, the energy and the momentum is conserved, thus, $E_f = E_i$ and

$$\vec{k}_2 = \vec{k}_1 + \vec{k}_3 - \vec{k}. \tag{6}$$

The electron-electron scattering processes are described by[17,45,53]

$$\Gamma_{\text{el-el}} = \frac{2\pi}{\hbar} \sum_{\vec{k}_1} \sum_{\vec{k}_3} \mathcal{F} M_{\text{ee}}^2(\Delta k,\kappa)\delta(E_i - E_f), \tag{7}$$

where

$$\mathcal{F} = f_1 f_3(1-f)(1-f_2) - f f_2(1-f_1)(1-f_3)$$

determines with $f_i \equiv f(E_i,t)$ the collision functional ensuring the Pauli principle,

$$|M_{\text{ee}}(\Delta k,\kappa)|^2 = \left(\frac{e^2}{\epsilon_0 \Omega} \frac{1}{\Delta k^2 + \kappa^2}\right)^2 \tag{8}$$

the matrix element, κ the screening parameter, and $\Delta\vec{k} = \vec{k} - \vec{k}_3$ the exchanged momentum. All of these properties are described in detail in Ref. 17. Assuming continuous energy eigenstates of the electron system, the collision integral can be rewritten to

$$\Gamma_{\text{el-el}} \approx \frac{\Omega^2}{(2\pi)^5 \hbar} \int d\vec{k}_1 \int d\vec{k}_3 \; \mathcal{F} M_{\text{ee}}^2 \; \delta(E_i - E_f), \tag{9}$$

which results in a six-dimensional integral. By assuming an isotropic system and spherical coordinates, two integrals over the azimuth angles vanish. Furthermore, the δ function cancels one integral and one integral is expressed analytically as $\mathcal{I} \equiv \int d\Delta k M_{\text{ee}}^2(\Delta k,\kappa)$. By substituting the momentum to an energy using (4), we find

$$\Gamma_{\text{el-el}} = \frac{\Omega^2 \pi^3}{8\hbar k} \int dE_1 \int dE_3 \; \frac{D(E_1)}{k_1} \frac{D(E_2)}{k_2} \frac{D(E_3)}{k_3} \mathcal{I}\, \mathcal{F}\, \Xi_{\text{ee}}, \tag{10}$$

where Ξ_{ee} is a step function, which enters due to the assumption of isotropy: it checks explicitly if the momentum is conserved during a collision process. To derive this function Ξ_{ee}, we square Eq. (6) resulting in

$$\mu = \frac{k^2 + k_2^2 - k_1^2 - k_3^2 + 2k k_2 p}{2 k_1 k_3} \tag{11}$$

with $\mu = \cos(\angle(\vec{k}_1,\vec{k}_3)) \in [-1,1]$ and $p = \cos(\angle(\vec{k},\vec{k}_2)) \in [-1,1]$. This criterion is simplified to

$$|a| \leqslant 1 + b \tag{12}$$

with $a = (k^2 + k_2^2 - k_1^2 - k_3^2)/(2k_1 k_3)$ and $b = k k_2/(k_1 k_3)$. Hence, Ξ_{ee} is unity when the criterion (12) holds and vanishes otherwise. In the case of a free-electron gas, Ξ_{ee} is always one because for $E(\vec{k}) \propto k^2$ the numerator of a vanishes, thus Eq. (12) is always fulfilled. However, for realistic materials, it is essential to determine Ξ_{ee} explicitly. With the aforementioned simplifications, we reduced the six-dimensional integral (9) to a two-dimensional integral (10), which minimizes the computational effort tremendously.

B. Electron-phonon-photon collisions

To describe the electron-phonon scattering processes we consider an electron with the energy E ending up within the energy state E_1. Meanwhile, a phonon within the Debye model with its energy $E_q = \hbar c_s q$ is emitted or absorbed. Here, c_s denotes the speed of sound of the longitudinal mode since only this mode contributes significantly to the electron-phonon coupling.[54] We simultaneously consider the absorption and emission of $|\ell|$ photons with energy $\hbar\omega$ in this scattering process, where a positive ℓ means emission and $\ell < 0$ means absorption. This leads to the energy balance $E_1 = E \pm E_q - \ell\hbar\omega$ and the momentum conservation

$$\vec{k}_1 = \vec{k} + \vec{q} \tag{13}$$

with the assumption that the momentum of the photons is negligible compared to the phonon momentum. The scattering processes can be expressed as a three-dimensional collision integral[55]

$$\Gamma_{\text{el-ph}} = \frac{2\pi}{\hbar} \sum_{\vec{q},\ell,\pm} M_{\text{ep}}^2(q,\kappa) J_\ell^2(\vec{\gamma}\vec{q}) \mathcal{F}^{\pm} \delta(E_1 - E \mp E_q + \ell\hbar\omega) \tag{14}$$

describing the change of the electron distribution function due to electron-phonon-photon collisions. Here, the collision functional has the form

$$\mathcal{F}^{\pm} = f_1(1-f)\left(g + \tfrac{1}{2} \pm \tfrac{1}{2}\right) - f(1-f_1)\left(g + \tfrac{1}{2} \mp \tfrac{1}{2}\right),$$

and the matrix element reads as[56]

$$M_{\text{ep}}^2(q,\kappa) = \frac{e^2}{2\epsilon_0 \Omega} \frac{E_q}{q^2 + \kappa^2}.$$

Transforming the sum of $\vec{q}$ in Eq. (14) into a spherical three-dimensional integral, the integral over the azimuth angle cancels because of the isotropy of the system. The Bessel function $J_\ell(\vec{\gamma}\vec{q}) \equiv J_\ell(e\vec{E}_L\vec{q}/m\omega^2)$ (Ref. 55) is replaced by an averaged Bessel function $\bar{J}_\ell^2(\gamma q) \equiv \frac{1}{2}\int_{-1}^{1} J_\ell(\gamma q \eta)^2 \, d\eta$ with $\eta = \cos[\angle(\vec{E}_L,\vec{q})]$ covering all angles between the laser field $\vec{E}_L$ and the exchanged momentum $\vec{q}$.

Substituting the integral of the polar angle into an electron momentum k_1 by exploiting the momentum conservation (13) and transforming the integral of q to an energy integral using (4) and introducing the Debye density of states of the phonon

system $D_{\mathrm{ph}}(E) = 9E^2/[(k_B T_D)^3 \Omega]$, we find

$$\Gamma_{\text{el-ph}} = \frac{\Omega \pi^3}{\hbar k} \int_0^{E_D} dE_q \sum_{\ell,\pm} \frac{D(E_1)}{k_1} \frac{D_{\mathrm{ph}}(E_q)}{q} \mathcal{F}^{\pm} M_{\mathrm{ep}}^2 \bar{J}_\ell^2 \Xi_{\mathrm{ep}} \,. \tag{15}$$

The upper limit for the integration is the Debye energy E_D, which is the maximum energy of a phonon in the Debye model. Due to the restriction of the momentum conservation, the function Ξ_{ep} equals unity when

$$\cos[\angle(\vec{k},\vec{q})] = \frac{q^2 + k^2 - k_1^2}{2kq} \in [-1,1] \tag{16}$$

is fulfilled, otherwise Ξ_{ep} vanishes. With (15), we derived the complete collision integral for the electron-phonon-photon collision changing the electron distribution $f(E,t)$.

C. Phonon-electron-photon collision

Here, we consider the same collision as in the previous section but concentrate on the influence on the phononic distribution. As in Ref. 17, we write

$$\Gamma_{\text{ph-el}} = 2\frac{1}{3}\frac{2\pi}{\hbar} M_{\mathrm{ep}}^2 \sum_{\vec{k}} \sum_{\ell} J_\ell^2(\vec{q}) \mathcal{F} \delta(E_i - E_f),$$

considering that both spin types couple to the longitudinal phonon mode. With similar simplifications as made in the evaluation of the electron-phonon collision term (15), we end up with

$$\Gamma_{\text{ph-el}} = \frac{\Omega \pi^3}{3\hbar q} M_{\mathrm{ep}}^2 \int dE \sum_{\ell} \bar{J}_\ell^2 \frac{D(E)}{k} \frac{D(E_1)}{k_1} \mathcal{F} \; \Xi_{\mathrm{ep}}. \tag{17}$$

Equation (17) is the counterpart of the integral for electron-phonon-photon collisions (15) determining the change of the phonon distribution function $g(E_q,t)$. With these both terms, our model describes the energy transfer from the electron into the phonon system.

D. Electron-ion-photon collision

In this work, we disregard the complete band structure resulting from a periodic potential but consider an effective one-band model of quasifree electrons. To account for the potential of the lattice ions we consider an additional collision term determining the absorption of photons by inverse bremsstrahlung.[17,53] An ion is considered to have an infinite mass compared to the electron mass, thus an arbitrary momentum $\Delta\vec{k}$ but no energy can be transferred to a colliding free electron. This scattering process is written as

$$\Gamma_{\text{absorb}} = \frac{2\pi}{\hbar} \sum_{\Delta\vec{k}} \sum_{\ell} M_{\mathrm{ee}}^2 J_\ell^2(\vec{\gamma}\Delta\vec{k}) \mathcal{F} \delta(E_i - E_f) \tag{18}$$

with $\mathcal{F} = f_1(1-f) - f(1-f_1)$. Similar to the simplifications performed before, we transfer (18) into spherical coordinates and find

$$\Gamma_{\text{absorb}} = \frac{\Omega \pi}{2\hbar k} \int d\Delta k \sum_{\ell} \frac{D(E_1)}{k_1} \; \Delta k \; M_{\mathrm{ee}}^2 \bar{J}_\ell^2(\gamma \Delta k) \mathcal{F} \; \Xi_{\mathrm{ei}}. \tag{19}$$

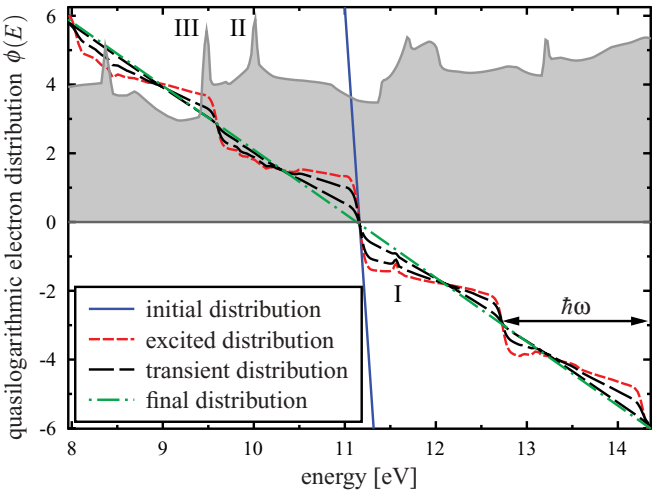

FIG. 2. (Color online) Quasilogarithmic transient distribution function $\phi(E)$ [Eq. (21)] of aluminum after a laser irradiation of 0.12 mJ/cm^2. The transient distributions are shown for 17 and 40 fs. Background: The density of states in arbitrary units.

The step function Ξ_{ei}, ensuring momentum conservation, equals Ξ_{ep} in Eq. (16) when replacing q with the exchanged momentum Δk.

III. RESULTS

We solve the Boltzmann equation (2) for three different materials: aluminum, gold, and nickel. We chose aluminum since the density of states is similar to that of a free-electron gas[39] (see background of Fig. 2) and therefore allows a comparison to the results of Ref. 17. In striking contrast, gold and nickel have strong peaks in the DOS,[39] which can be seen in the background of Figs. 3 and 4, respectively. For nickel, the peaks are directly located at, and for gold they are 2 eV below, the Fermi energy.

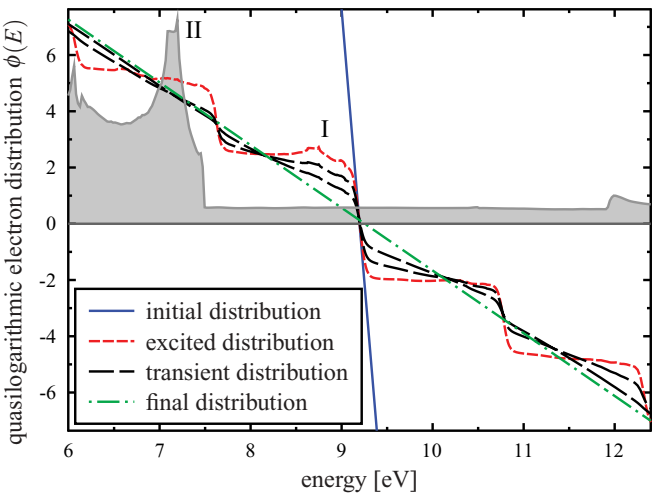

FIG. 3. (Color online) Quasilogarithmic transient distribution function (21) of gold after a laser irradiation of 0.12 mJ/cm^2. The transient distributions are shown for 40 and 100 fs. Background: The density of states in arbitrary units.

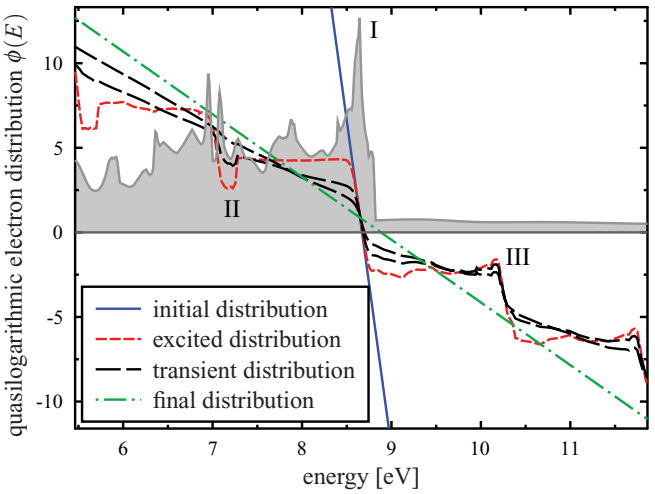

FIG. 4. (Color online) Quasilogarithmic transient distribution function (21) of nickel after a laser irradiation of 0.12 mJ/cm^2. The transient distributions are shown for 80 and 160 fs. Background: The density of states in arbitrary units.

As input parameters, three values are required and are summarized in Table I: the speed of sound c_s, the volume of the unit cell Ω, and the Fermi energy E_F. The Fermi energy is used to determine the initial chemical potential at a given finite temperature T_e by solving the implicit integral equation $n_e(T_e) = n_e(T_e = 0)$. The density $n_e(T_e)$ is given by Eq. (3b) by setting $B(E)$ to unity. As a fourth input parameter, the DOS $D(E)$ is needed, which is taken from Ref. 39. The Debye energy E_D in Table I has been derived from the volume of the unit cell Ω.[17] The screening κ, which strongly influences the collision rates of the electrons and the electron-phonon coupling, is approximated isotropically:[14]

$$\kappa^2(t) = \frac{e^2}{\epsilon_0} \int dE\ D(E) \frac{df(E,t)}{dE}. \tag{20}$$

The values of the screening in Table I are calculated with a Fermi distribution depending on electron temperature T_e. In the nonequilibrium case, when $f(E,t)$ is the distribution of the excited electrons, the screening $\kappa(t)$ is calculated dynamically at each time step. Equation (20) is a generalization of the screening for a free-electron gas given in Ref. 58 and applied in Ref. 17. This more general form strongly depends on the density of states near the chemical potential since the derivative of the distribution function at this point is very high for temperatures below Fermi temperature. As Table I illustrates, the screening for gold and aluminum is almost constant for different temperatures. However, in the case of nickel, it deviates by a factor of 2 for our maximum considered excitation strengths ($\Delta T_e \sim 10^4$ K) since the chemical potential depends significantly on the electron temperature.

TABLE I. Material parameters of aluminum, gold, and nickel. The quantities indicated by asterisks are calculated: E_D follows from Ω and the screening κ is determined by Eq. (20). The screening κ at 300 K is used as initial condition for our simulations and the value for 10 000 K is given to illustrate the dependence on the temperature.

		Ref.	Al	Au	Ni
c_s	(m/s)	(57)	6420	3240	6040
Ω	(10^{-29} m^3)	(57)	1.661	1.695	1.094
E_F	(eV)	(39)	11.18	9.2	8.63
E_D	(meV)	(*)	64.4	32.3	69.6
$\kappa(T_e = 300\ \text{K})$	(10^{10} 1/m)	(*)	2.69	2.50	11.90
$\kappa(T_e = 10\,000\ \text{K})$	(10^{10} 1/m)	(*)	2.95	3.05	5.78

The laser was chosen to be rectangular in time ($\tau_L = 10$ fs) at a wavelength of 800 nm, thus, $\hbar\omega = 1.55$ eV. The pulse duration is very short to reduce both changes in optical parameters[59] and thermalization of the electron system during the irradiation. For a clear illustration of our findings, we neglect any bandwidth of the photon energy. The (absorbed) excitation strength was varied from 0.013–0.65 mJ/cm^2 which corresponds to electric fields of $1–7\times10^8$ V/m. In this work, we assumed $\ell \leqslant 2$ (one- and two-photon absorption) for all materials since the difference to the absorbed energy with $\ell = 3$ was less than 1%. Initially, electrons and phonons are kept at room temperature $T_0 = 300$ K.

A. Excitation of the electron system

In the following, we investigate the influence of the excitation process on the electron distribution. We suppress the interaction with the phonons to store the absorbed energy of the laser field in the electron system and to concentrate on the dynamics of the electrons. To analyze the transient electron distribution $f(E,t)$ in detail, we chose a quasilogarithmic representation[17]

$$\phi[f(E,t)] = -\ln[1/f(E,t) - 1]. \tag{21}$$

The main benefit is that in thermal equilibrium, when $f(E,t)$ equals a Fermi distribution, $\phi(E)$ is linear in E with its root at the chemical potential and its slope is antiproportional to the electron temperature (see Fig. 2, initial and final distribution). A deviation from the linear behavior is an indication of a nonequilibrium state (Fig. 2, excited distribution). In contrast to a pure logarithmic representation, we also have insight into the dynamics below the chemical potential, i.e., *holes*. In Figs. 2–4, the initial distribution at 300 K, the distribution directly after the laser irradiation at $t = \tau_L$, the thermalized distribution function after $t = 2$ ps, and two selected transient distributions are depicted for the three materials under study.

In Fig. 2, the dynamics of the electron gas in laser-irradiated aluminum is shown. The initial electron distribution is disturbed by the laser excitation and steps with exactly the width of the photon energy $\hbar\omega$ are created: Due to the Pauli blocking, only the electrons in the energy interval $[\mu - \hbar\omega, \mu]$ may overcome the Fermi edge and establish the first two centered steps, the holes directly below and the excited electrons directly above μ. The excited electrons may again absorb photons creating the second step and so forth (see Ref. 17 for details). This steplike behavior has also been observed experimentally in gold.[4] In Fig. 2, a peak above the Fermi edge is observed in the excited electron distribution (I). It is a direct result from the density of states since one-photon energy below this peak a strong maximum in the density of states (II) is observed. In contrast, another peak (III) in the density of states at $E - \mu = 1.67$ eV $> \hbar\omega$ is not clearly

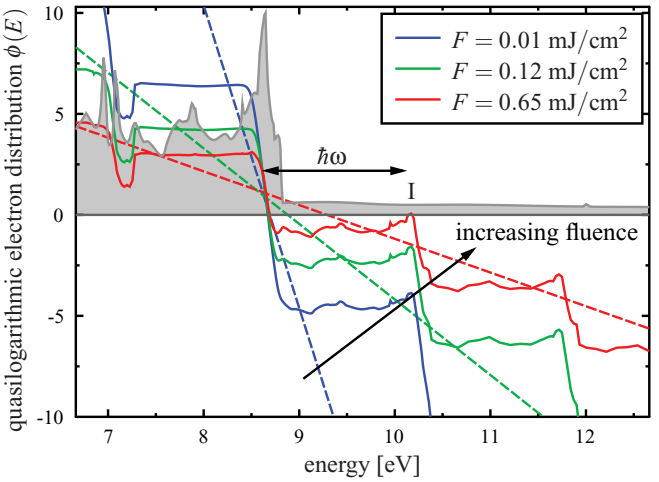

FIG. 5. (Color online) Quasilogarithmic electron distribution (21) of nickel for different excitation strengths directly after the laser irradiation $t = 10$ fs. The excited (solid line) as well as the thermalized (dashed line) distributions are depicted.

mirrored in the excited distribution function due to the Pauli blocking.

Similar effects are observed in gold (Fig. 3). The transient distribution functions have some hillocks (I) below the Fermi edge resulting from the large amount of d electrons (II) located $\approx$2 eV below the Fermi energy. These d electrons are excited by the laser to higher energies. Due to Pauli's principle, the resulting hillock is less pronounced as the density of states would suggest.

The DOS in nickel has the largest impact on the transient electron distribution (Fig. 4) since a vast amount of d electrons are located directly at the Fermi energy (I). Due to a lot of free places around μ, the scattering probability is increased and a large amount of holes is left at $E = \mu - \hbar\omega$ (II). Moreover, the large amount of electrons at the Fermi energy absorbs the photons and creates a hillock (III) above the chemical potential.

In Fig. 5, we study the influence of different excitation strengths on the electron distribution in nickel. The figure depicts the nonequilibrium distribution directly after the laser excitation as well as the equilibrium distribution function for different absorbed fluences. The nonequilibrium distribution shows a peak at one photon energy above the Fermi edge (I), which for the highest applied fluence even becomes positive. This strong excitation has a large influence on the electron-phonon coupling as will be shown in Sec. III C.

In Fig. 6(a), the absorbed energy of the electron system after the laser pulse $\delta u_e = u_e(t = \tau_L) - u_e(t = 0)$ with

$$u_e(t) = \int D(E) f(E,t) E \, dE \tag{22}$$

is plotted as a function of the laser fluence for aluminum, gold, and nickel. The corresponding temperature after the thermalization process depends not only on the absorbed energy, but also on the particular DOS and is shown in Fig. 6(b). The dependence of the absorbed energy on the laser fluence is almost linear, as the dominating term in the Taylor series of the averaged Bessel function $\bar{J}_1$ in Eqs. (15) and (19) is quadratic in the laser field, i.e., for the given laser pulse shape

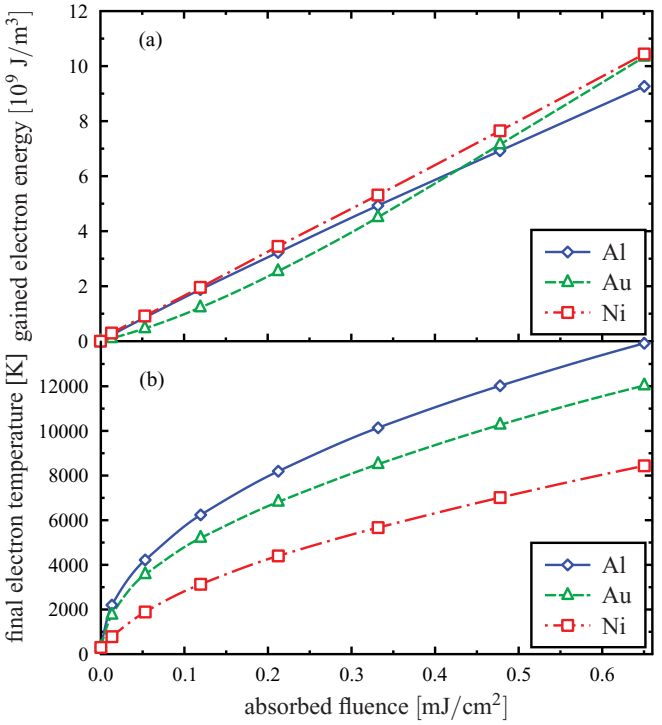

FIG. 6. (Color online) The internal energy gained by the electron system directly after the laser irradiation depending on the fluence (a). After the thermalization process (without the cooling of the phonons), a final electron temperature is reached which is plotted in (b).

linear in fluence. Additionally, the multiphoton absorption is often negligible in metals since $\bar{J}_2 \ll \bar{J}_1$. However, for gold, the linear dependence between fluence and absorbed energy slightly deviates, as multiphoton absorption comes into play. The strong peak in the DOS of gold [Fig. 3 (II)], which is 1.3 $\hbar\omega$ below the Fermi energy, facilitates a higher-order absorption process.

This large amount of d electrons in gold also has a large influence on the absorption properties for different photon energies. In Fig. 7, the gained electron energy in dependence of the photon energy or laser wavelength, respectively, is depicted. For aluminum and nickel, the energy decreases with increasing photon energy since ω enters in the denominator of the argument of the averaged Bessel function and therefore a higher photon energy $\hbar\omega$ leads to a reduced absorption probability. For gold, a conspicuous deviation from this behavior is observed when the photon energy exceeds 2 eV. This is exactly the characteristic absorption edge of the d electrons which for higher photon energies may be excited in a one-photon process directly across the Fermi level.

B. Thermalization of the electron system

The two-temperature model assumes implicitly that the electrons are in thermal equilibrium and a well-defined temperature characterizes the whole electron system. However, we showed in the last section that shortly after an ultrashort laser excitation this assumption is not valid. In the further course, a process called thermalization drives the electron system back into a new equilibrium state with a distinct temperature and chemical potential. The latter has to be considered carefully

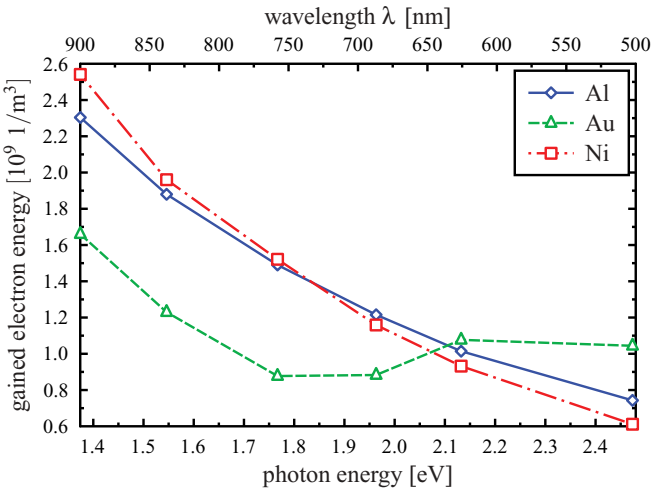

FIG. 7. (Color online) The absorbed energy in the electron system after the laser irradiation at different wavelengths and a constant fluence.

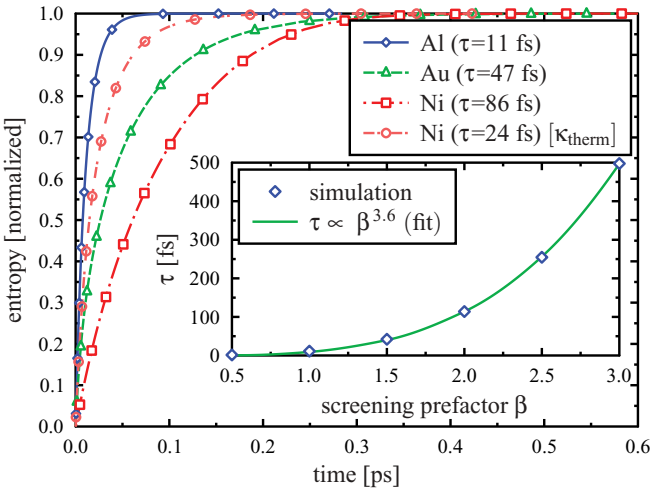

FIG. 8. (Color online) Transient entropy for the three considered materials aluminum, gold, and nickel. The absorbed fluence is 0.12 mJ/cm^2 Inset: The dependence of the thermalization time τ on the screening for the example of nickel. We changed the screening by a prefactor β: $\kappa'(t) = \beta \times \kappa(t)$.

as well since it influences the electron screening and the electron-phonon coupling as will be shown below, and plays an important role, for instance, in ultrafast magnetization dynamics.[48] To estimate whether and when the assumptions of the TTM hold, we analyze the thermalization process. It can be characterized by a certain thermalization time τ, which depends on excitation type, excitation strength, and material properties.[4] As in Sec. III A, we suppress the interaction with the phonons, thus the energy density in the electron system (22) is constant during the thermalization process.

Figures 2–4 illustrate the evolution of the excited electron distribution towards a thermalized one. The final quasilogarithmic distribution $\phi(E)$ [c.f. Eq. (21)] at 2 ps after laser excitation is depicted in the respective green dashed-dotted curves. For all three materials, it is again linear as the initial one, indicating that the system is thermalized. However, compared to the initial distribution, it has lower slope, signifying a higher temperature than in the initial state.

We exploit the second law of thermodynamics stating that the entropy of an isolated system increases or, in the case of thermal equilibrium, remains constant. Thus, we trace the transient entropy of the electron system[60]

$$S = -\int dE\ D(E)\,[f \ln(f) + (1-f)\ln(1-f)] \quad (23)$$

to extract the characteristic time τ of thermalization. The second term $(1-f)$ accounts for the holes and is essential to compute the complete electron entropy.

Figure 8 depicts the normalized transient entropies of the three metals after irradiation with a laser described above (800 nm, 10 fs duration) and an absorbed fluence of 0.12 mJ/cm^2. The curves fit well to an exponential function and the characteristic time is identified with the thermalization time τ. For aluminum, gold, and nickel, we find for the same laser fluence $\tau = 11$ fs, $\tau = 47$ fs, and $\tau = 86$ fs, respectively. As already claimed, the thermalization strongly depends on the distinct material. Aluminum thermalizes fast, while nickel and gold are much slower. Primarily, this is due to both the screening parameter κ and the density of states. First, we analyze the influence of the screening parameter on the thermalization process. For that we assume different artificial screening parameters in nickel, keeping all other features of the respective simulation as before. The resulting thermalization time is shown in the inset of Fig. 8 in dependence on the assumed screening parameter $\kappa'(t) = \beta \times \kappa(t)$, which was obtained by multiplying the screening according to Eq. (20) with factors β between 0.5 and 3.0.

An empirical relation $\tau \propto \beta^n$ has been fitted to our results. We expect a result around $n = 4$ since the electron-electron collision integral in Eq. (7) with (8) depends on $(\Delta k^2 + \kappa^2)^{-2}$, which can be estimated to κ^{-4} since the transferred momentum Δk is commonly smaller than the screening κ. Indeed, our fit delivers $n = 3.6$, thus, a thermalization time $\tau \propto \kappa^{3.6}$, showing that the screening has a significant influence on the thermalization process.

Figure 9 depicts the transient screening according to Eq. (20) of all three materials for a fluence of 0.65 mJ/cm^2 under nonequilibrium and equilibrium conditions. In the nonequilibrium case, we directly applied Eq. (20) with the transient nonequilibrium distribution function $f(E,t)$. To compare with equilibrium conditions, we calculate κ through Eq. (20) choosing at each moment the corresponding thermalized Fermi distribution providing the same internal energy and density as the nonequilibrium distribution. For gold and aluminum, the screening is almost constant and nonequilibrium effects play a minor role. For nickel, the temperature dependence as well as the nonequilibrium effects of the screening are tremendous. In this context, we simulate nickel by applying a screening under equilibrium conditions and compared it with the nonequilibrium case (Fig. 8). Both results deviate strongly, hence, it is essential to apply Eq. (20) dynamically rather than using equilibrium approximations such as Thomas Fermi or Debye screening without any information about the electron distribution.

Figure 9 and Table I show also that aluminum and gold feature a similar screening. Therefore, we expect a similar

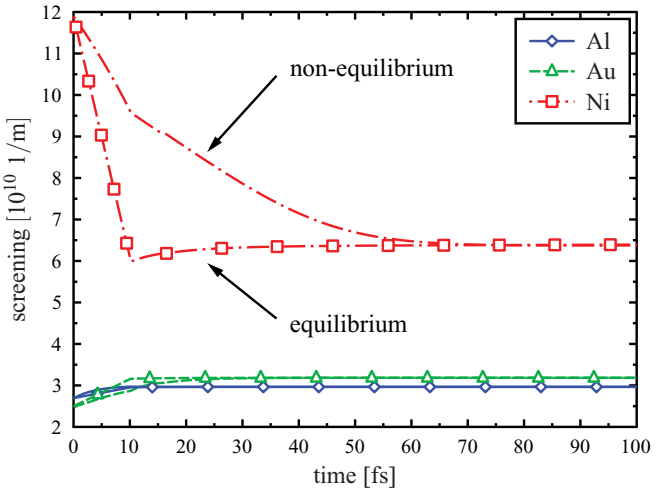

FIG. 9. (Color online) The transient screening under nonequilibrium and equilibrium conditions for aluminum, gold, and nickel. The laser fluence was chosen to 0.65 mJ/cm^2. Here, electron-phonon collisions are considered.

thermalization time. However, the characteristic time for the entropy increase in Fig. 8 pronounces differences. The reason is that the density of states of both materials differ. As Eq. (10) and Ref. 15 suggest, the density of states influences the thermalization primarily around the Fermi level or, more precisely, the chemical potential

$$1/\tau \propto D(E \approx \mu)^3.$$

Most of the collisions occur in this region as the collision functional $\mathcal{F}$ in Eq. (10) has its maximum around μ.

However, the thermalization time depends not only on the material properties but on the excitation strength as well. Figure 10 depicts the thermalization time, which is extracted from the entropy evolution in dependence on the absorbed fluence. The thermalization time decreases strongly with the fluence, ranging from picoseconds to less than 10 fs with increasing intensity. This indicates that for a higher energy

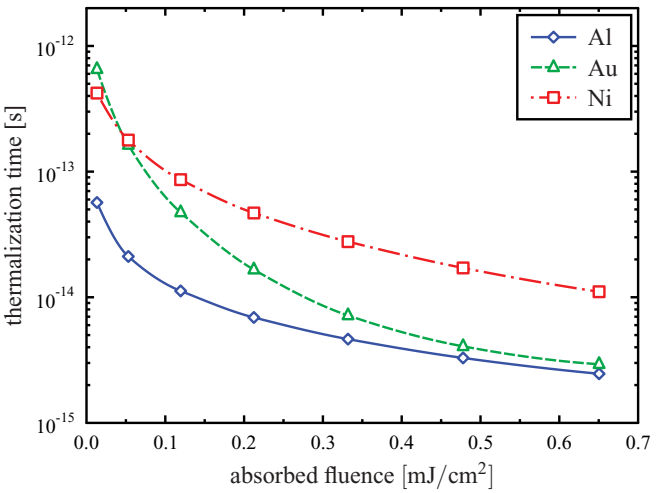

FIG. 10. (Color online) The thermalization time τ after excitation with a 10-fs laser pulse of 800 nm. The thermalization time was extracted from the evolution of the entropy [see Eq. (23)].

deposited in the electron system, the equilibrium state is reached faster due to the increased phase space of the electrons. From Fermi-liquid theory, an expression has been found to determine an energy-dependent collision rate of an excited electron with energy E within a thermalized electron bath at temperature T_e (Refs. 61–63):

$$\frac{1}{\tau_{ee}(E,T_e)} = \frac{\pi^2\sqrt{3}}{128}\frac{\omega_p}{E_F^2}\frac{(\pi k_B T_e)^2 + (E-E_F)^2}{e^{-(E-E_F)/k_B T_e}+1}, \quad (24)$$

where $\omega_p = \sqrt{\frac{n_e e^2}{m\varepsilon_0}}$ determines the plasma frequency. We should clearly distinguish between the collision time of *one* excited electron in a thermalized electron bath [see Eq. (24)] and the time scale in which the whole laser-excited system is equilibrated [here determined by the transient entropy of Eq. (23)]. The collision time of one excited "hot" electron is strongly energy dependent, whereby the above-discussed thermalization time τ of the complete excited electron system is an averaged quantity. It is instructive to compare the thermalization time, obtained through the transient entropy according to Eq. (23), with the electron collision rate of Eq. (24) since this assumption is often applied in the literature.[6,64,65] To that end, we approximate Eq. (24) for electrons with energies $(E - E_F) \ll k_B T$ since the integrand of Eq. (23) has its maximum at the Fermi edge. A simple dependence of the collision time on the electron temperature is found:

$$\frac{1}{\tau_{ee}(T_e)} = \frac{\pi^4 k_B^2\sqrt{3}}{256}\frac{\omega_p}{E_F^2}T_e^2 \quad (25)$$

$$\equiv A T_e^2 \ . \quad (26)$$

To estimate the validity of this approximation with the help of our kinetic approach, we extract the final electron temperature, which will be reached after the excitation and thermalization process ($t \gtrsim 2$ ps) from the distribution function $f(E,t)$. Here, this temperature is constant since no energy transfer to the phonons is taken into account. We follow the thermalization process to this temperature through the analysis of the transient entropy according to Eq. (23).

In Fig. 11, we compare Eq. (26) to our extracted thermalization times of the transient entropy by using a double-logarithmic representation. Thus, we expect a linear behavior with a negative slope of two which is in good agreement for aluminum, however, for gold and nickel this estimation is less appropriate. This is due to the strong simplifications which are made in Eqs. (24) and (25): The density of states was assumed to be free-electron like, the screening has not been taken explicitly into account, and only electrons at the Fermi edge are considered. Figure 11 indicates a smaller exponent in Eq. (26) for nickel, which was also proposed in Ref. 20.

The thermalization prefactors A found in literature diverge strongly (see Table II), and in general this parameter is barely investigated. We compare them with those obtained from Eq. (25), and there are remarkable differences as well, again indicating that Eq. (25) is only a rough approximation. Nevertheless, Eq. (26) gives an adequate estimate for the temperature dependence of the thermalization time in the considered range of excitations and is often applied in the context of electrical or heat conduction.[6,27,33,66,68,69] Therefore, we fitted the thermalization factor A to all our

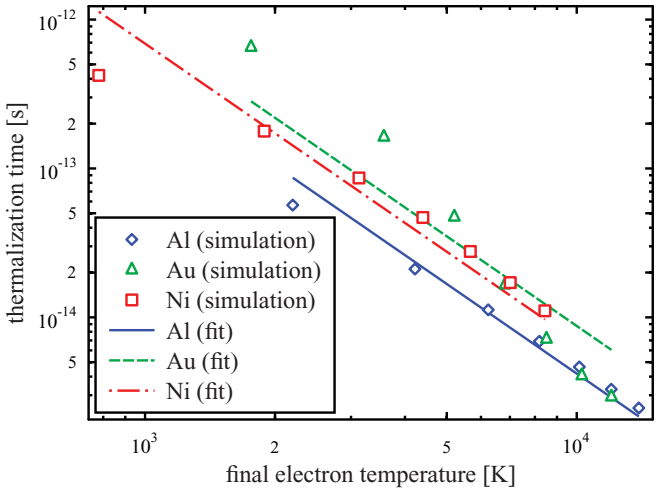

FIG. 11. (Color online) The thermalization times, extracted from the transient entropy [see Eq. (23)], are plotted against the final electron temperatures after the thermalization process. In the double-logarithmic representation, the lines are linear fits of Eq. (26) to our data points. The extracted parameters A are listed in Table II.

simulation results, and summarize the extracted A in Table II.[72]

C. Electron-phonon coupling

In the previous section, we have shown that the electron system thermalizes within a characteristic thermalization time τ in the range of some femtoseconds to picoseconds depending on the irradiation strength. Applying the two-temperature model for times shorter than τ is thus questionable. Nevertheless, in many applications, the TTM was successfully applied after an ultrashort laser excitation .[9–11,33] In particular, for high fluences, when thermalization is rather fast (see Fig. 10), this can be justified. However, it has been shown that the heat transfer from nonequilibrium electrons to the lattice is delayed in comparison to the thermalized electron gas.[17] This can be to some extent interpreted as a reduced electron-phonon coupling parameter α in Eq. (1). In general, a constant electron-phonon coupling as often applied in the literature is a strong simplification, in particular, when the effect of the strong deviation from a free-electron-gas like DOS comes into play.[39] It was shown in Ref. 70 that the application of a temperature-dependent coupling strength leads to a better agreement between experimental observation and theoretical simulation. Moreover, the temperature dependence of the

TABLE II. The prefactor A in (10^6 K^{-2} s^{-1}) for different materials. The last row lists the values from the literature.

	Al	Au	Ni
Simulation (Fig. 11)	2.39	1.14	1.45
Fermi liquid [Eq. (25)]	0.94	2.62	3.55
Literature	0.91 (66)	12.0 (27)	1.4 (27)
	0.6 (expt) (65)	45.7 (66)	5.9 (67)
	14.2 (theor) (65)	11.8 (33)	
	3.76 (68)	3.67 (9)	

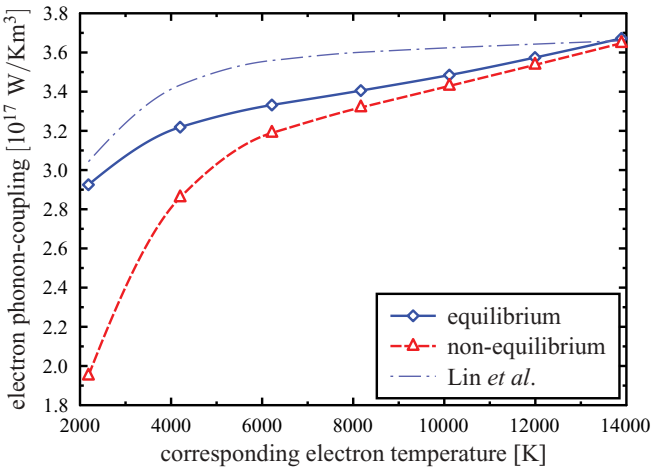

FIG. 12. (Color online) Electron-phonon coupling of aluminum for different excitation strengths corresponding to electron temperatures according to Fig. 6. The coupling factors for nonthermalized electrons, thermalized electrons, and the comparison to Lin *et al.* are depicted.

coupling parameter may directly influence the finally observed material modification.[21]

In this work, we analyze the strength of the electron-phonon coupling after ultrafast laser excitation for the three materials aluminum, gold, and nickel. To that end, we consider now the influence of the phonon system by including the collision rates Eqs. (15) and (17) in our calculation. In the case that T_e and T_p are defined, the coupling factor α can be extracted from the definition of the TTM (1) after irradiation [i.e., when $S(t)=0$] and neglecting heat conduction:

$$\alpha = \left.\frac{du_e/dt}{T_p - T_e}\right|_{t=\tau_L}. \tag{27}$$

The internal energy u_e is given in Eq. (22). We evaluate the electron-phonon coupling directly at the end of irradiation. Generally, and as shown in the last section, the system is in nonequilibrium by that time. For the calculation of the electron-phonon coupling through Eq. (27) under nonequilibrium conditions, we therefore determine T_e as the temperature the electron system would reach after thermalization in the case of no heat exchange (Fig. 6). The temperature T_p of the phonon system can be determined in a similar manner.[73] We compare this nonequilibrium case with the equilibrium one, which is given by an equilibrium electron system and a phonon system at the same respective internal energies. The electron-phonon coupling parameters α resulting from our simulations for the equilibrium and the nonequilibrium condition are depicted in Figs. 12–14. Additionally, the results from Lin *et al.*[39] calculated under equilibrium conditions are presented.

First, we analyze the electron-phonon coupling in the equilibrium case, i.e., the blue solid lines in the respective figures. For aluminum and gold (Figs. 12 and 13), the electron-phonon coupling increases with increasing laser intensity, i.e., electron temperature. This can be explained directly: The phonon energies $E_q \leqslant E_D$ are typically in the order of several meV. Hence, due to Pauli's principle, only electrons in narrow energy interval ($\approx k_B T_e$) around the chemical potential

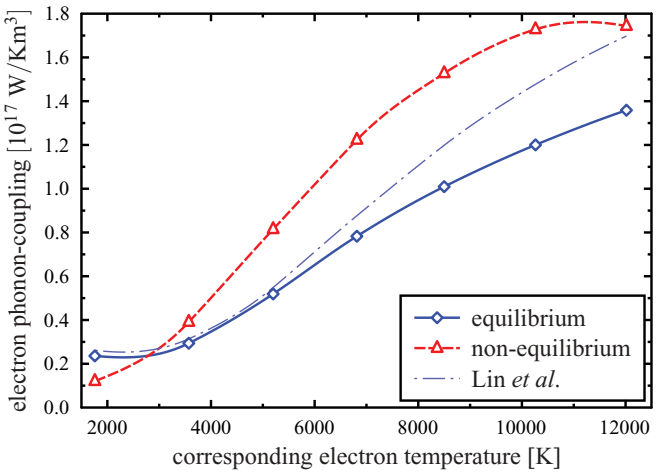

FIG. 13. (Color online) Electron-phonon coupling of gold for different excitation strengths corresponding to electron temperatures according to Fig. 6. The coupling factors for nonthermalized electrons, thermalized electrons, and the comparison to Lin *et al.* are depicted.

contribute to the electron-phonon collisions. With increasing electron temperature, more and more electrons couple to the phonons because the interaction interval $k_B T_e$ increases. Therefore, the coupling parameter α is expected to increase with the electron temperature.

In striking contrast, for nickel the behavior of the electron-phonon coupling in the equilibrium case is vice versa; the blue solid line in Fig. 14 decreases with increasing temperature. This behavior is even more unexpected since, as Table I shows, the screening decreases with increasing temperature and should thus lead to an increased coupling. However, the large amount of d electrons located exactly at the Fermi edge (see background in Fig. 5) complicates the physics: The chemical potential $\mu(T_e)$ depends significantly on the temperature (see roots of the initial and final distribution

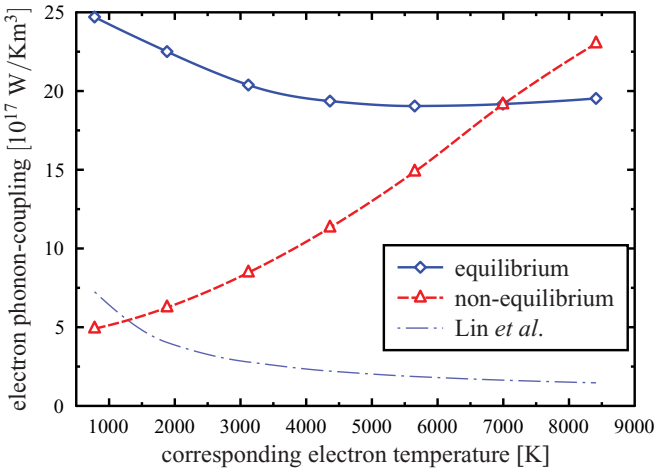

FIG. 14. (Color online) Electron-phonon coupling of nickel for different excitation strengths corresponding to electron temperatures according to Fig. 6. The coupling factors for nonthermalized electrons, thermalized electrons, and the comparison to Lin *et al.* are depicted.

in Fig. 5). On that account, by increasing the electron temperature, and therefore the chemical potential as well, a dramatic decrease in the electron occupation probability $f(E,t) \times D(E)$ around the chemical potential leads to the observed counterintuitive behavior.

We compare our results to those presented in Lin *et al.*[39] for thermalized electron gases and notably we find a quite good agreement for aluminum and gold, though, the authors utilize the moment of the spectral function $\lambda\langle\omega^2\rangle$ from experimental data. In contrast, our approach relies only on a few material parameters (see Table I) and the density of states, *without* any experimental input. In the case of nickel, our approach and that of Lin *et al.* leads to the same qualitative behavior, however, shifted to a higher absolute coupling in our case. We suppose that some assumptions in Ref. 39 do not correspond to our model: The authors of Ref. 39 introduced the Eliashberg function and further assumed a constant matrix element M_{ep} to simplify the complicated integrals we solved numerically. In addition, they assume a constant screening, implicitly included in the experimentally obtained moment of the spectral function $\lambda\langle\omega^2\rangle$. In this work, we found that the screening parameter has a large influence on the results and calculated it in dependence on temperature. On the other hand, our model, considering only the density of states instead of the complete band structure, could have neglected some mechanisms such as possibly important interband transitions which are, of course, covered by the experiment and implied in $\lambda\langle\omega^2\rangle$. To investigate this issue, *ab initio* calculations with the detailed electron band structure become necessary.

Let us now analyze the electron-phonon coupling under nonequilibrium conditions, i.e., in this case after 10 fs of laser irradiation at 800 nm. The coupling parameters α shown as red dashed lines in Figs. 12–14, respectively, strongly differ from the equilibrium case. For aluminum (Fig. 12), the electron-phonon coupling is suppressed for low temperatures and conforms for higher temperatures. This is the same effect as explained in Ref. 17 [Figs. 5(b) and 6(b) therein] for the case of a free-electron gas since the weakly excited distribution function behaves in the region $\pm E_D$ like an unexcited distribution around the chemical potential. The electron-phonon collisions mainly take place in this region and therefore the coupling is reduced as compared to the thermalized case. For higher excitations, the thermalization is faster (see previous section), thus, the coupling in nonequilibrium resembles the equilibrium case. As experimentally confirmed,[9] the electron-phonon coupling in gold under nonequilbrium conditions (Fig. 13) is suppressed for the same reasons in the case of very low excitation when s electrons close around the chemical potential determine the relaxation behavior. However, for higher intensities, the nonequilibrium coupling factor even *exceeds* the equilibrium case as has also been observed experimentally.[71] This is due to the d electrons which are excited with an increasing probability for increasing intensity (i.e., increasing irradiation strength in our case). These electrons then also contribute to the electron-phonon coupling and therefore speed up the coupling. Strikingly, in nickel the nonequilibrium coupling under nonequilibrium conditions behaves vice versa than in the equilibrium case (see Fig. 14). For low excitations, the coupling is suppressed and the same explanation as for aluminum holds. Moreover,

the shift of the chemical potential determining the behavior under equilibrium conditions is not completed directly after excitation. For higher fluences, the particular DOS of nickel leads to an excitation of a large number of d electrons above the chemical potential. This is reflected in a large occupation probability in the interval $[\mu,\mu+\hbar\omega]$ in Fig. 5. Within this energy interval, the Pauli principle is powerless and the electrons scatter in a large phase space which increases the electron-phonon coupling even above the equilibrium condition. Also, the screening deviates dramatically in both cases (compare Fig. 9 which was calculated for the largest excitation strength shown in Fig. 5). However, the larger screening under nonequilibrium conditions has a minor influence here. In contrast to noble metals, experimental studies on transition metals are rare.[20] The increase of electron-phonon coupling with excitation strength under nonequilibrium conditions as reported here for nickel has, to our knowledge, not yet been observed experimentally. However, large deviations resulting from different measurements were reported,[20] which may be due to different nonequilibrium states upon ultrafast excitation. We hope that our study stimulates further experimental efforts on this topic.

IV. SUMMARY

In this work, we analyzed the excitation and thermalization of electrons during and after an ultrashort laser irradiation and, additionally, the influence of a nonequilibrium electron distribution on electron-phonon coupling. We derived appropriate Boltzmann collision integrals including the density of states explicitly within an effective one-band model. For three materials, aluminum, gold, and nickel, we first analyzed the excitation by an ultrashort laser pulse and found that the properties of the density of states play a significant role. For aluminum, the behavior resembles that of a free-electron gas as has been studied in Ref. 17. In gold, electrons are excited from the d bands above the chemical potential changing the excited electron distribution drastically. In nickel, the particular large density of states directly at the Fermi edge leads to a very high occupation probability above the Fermi edge upon excitation, which influences both thermalization and electron-phonon coupling.

We extracted thermalization times for certain laser parameters and have studied the influence of screening on the thermalization. We showed that a nonequilibrium electron distribution may strongly change the screening and thus thermalization dynamics. Furthermore, we analyzed the approximation that the inverse thermalization time depends on the square of the electron temperature which will be reached after the thermalization process. We found that this assumption provides only a rough estimation since the screening and density of states are not considered explicitly.

We have studied the electron-phonon coupling for different excitation strengths. For a thermalized electron gas, the electron-phonon coupling was found to increase with increasing electron temperature for aluminum and gold. However, for nickel the coupling decreases due to the large amount of d electrons at the Fermi edge. For the nonequilibrium case, the coupling is expected to be lower due to the reduced phase space the electrons can scatter in. We showed that this is indeed the case for low excitations for all three studied materials. For higher irradiation strengths, the coupling in aluminum behaves similar to equilibrium due to the fast thermalization. In gold and in nickel, the electron-phonon coupling is strengthened due to the excited d electrons.

We conclude that for low excitations the two-temperature model does not hold directly after the laser irradiation due to the slow thermalization. However, it could be applied for high irradiation intensities for free-electron-like metals. For more complicated metals, as for instance for gold or nickel, the corresponding parameters should be examined carefully for the particular irradiation conditions and more advanced models become necessary.

ACKNOWLEDGMENT

Financial support of the Deutsche Forschungsgemeinschaft through the Emmy Noether Project RE 1141/11-1 "Ultrafast Dynamics of Laser-excited Solids" is gratefully acknowledged.

*bmueller@physik.uni-kl.de

[1] D. Bäuerle, *Laser Processing and Chemistry*, 4th ed. (Springer, Berlin, 2011).
[2] A. Vogel and V. Venugopalan, Chem. Rev. **103**, 577 (2003).
[3] C. Frischkorn and M. Wolf, Chem. Rev. **106**, 4207 (2006).
[4] W. S. Fann, R. Storz, H. W. K. Tom, and J. Bokor, Phys. Rev. B **46**, 13592 (1992).
[5] W. S. Fann, R. Storz, H. W. K. Tom, and J. Bokor, Phys. Rev. Lett. **68**, 2834 (1992).
[6] X. Y. Wang, D. M. Riffe, Y.-S. Lee, and M. C. Downer, Phys. Rev. B **50**, 8016 (1994).
[7] N. A. Inogamov, V. V. Zhakhovskii, S. I. Ashitkov, V. A. Khokhlov, Y. V. Petrov, P. S. Komarov, M. B. Agranat, S. I. Anisimov, and K. Nishihara, Appl. Surf. Sci. **255**, 9712 (2009).
[8] D. K. Efetov and P. Kim, Phys. Rev. Lett. **105**, 256805 (2010).
[9] R. H. M. Groeneveld, R. Sprik, and A. Lagendijk, Phys. Rev. B **51**, 11433 (1995).
[10] J. Hohlfeld, S.-S. Wellershoff, J. Güdde, U. Conrad, V. Jähnke, and E. Matthias, Chem. Phys. **251**, 237 (2000).
[11] M. Bonn, D. N. Denzler, S. Funk, M. Wolf, S. Svante Wellershoff, and J. Hohlfeld, Phys. Rev. B **61**, 1101 (2000).
[12] M. Lisowski, P. A. Loukakos, U. Bovensiepen, J. Stähler, C. Gahl, and M. Wolf, Appl. Phys. A: Mater. Sci. Process. **78**, 165 (2004).
[13] C.-K. Sun, F. Vallée, L. H. Acioli, E. P. Ippen, and J. G. Fujimoto, Phys. Rev. B **50**, 15337 (1994).
[14] N. Del Fatti, C. Voisin, M. Achermann, S. Tzortzakis, D. Christofilos, and F. Vallée, Phys. Rev. B **61**, 16956 (2000).
[15] R. Knorren, K. H. Bennemann, R. Burgermeister, and M. Aeschlimann, Phys. Rev. B **61**, 9427 (2000).
[16] A. V. Lugovskoy and I. Bray, Phys. Rev. B **60**, 3279 (1999).

[17]B. Rethfeld, A. Kaiser, M. Vicanek, and G. Simon, Phys. Rev. B **65**, 214303 (2002).
[18]P. J. van Hall, Phys. Rev. B **63**, 104301 (2001).
[19]N. Medvedev, U. Zastrau, E. Förster, D. O. Gericke, and B. Rethfeld, Phys. Rev. Lett. **107**, 165003 (2011).
[20]M. van Kampen, J. T. Kohlhepp, W. J. M. de Jonge, B. Koopmans, and R. Coehoorn, J. Phys.: Condens. Matter **17**, 6823 (2005).
[21]J. P. Colombier, F. Garrelie, N. Faure, S. Reynaud, M. Bounhalli, E. Audouard, R. Stoian, and F. Pigeon, J. Appl. Phys. **111**, 024902 (2012).
[22]V. Recoules, J. Clérouin, G. Zérah, P. M. Anglade, and S. Mazevet, Phys. Rev. Lett. **96**, 055503 (2006).
[23]S. M. Vinko, U. Zastrau, S. Mazevet, J. Andreasson, S. Bajt, T. Burian, J. Chalupsky, H. N. Chapman, J. Cihelka, D. Doria *et al.*, Phys. Rev. Lett. **104**, 225001 (2010).
[24]E. S. Zijlstra, F. Cheenicode Kabeer, B. Bauerhenne, T. Zier, N. Grigoryan, and M. E. Garcia, Appl. Phys. A: Mater. Sci. Process. (2012), doi: 10.1007/s00339-012-7183-0.
[25]B. Chimier, V. T. Tikhonchuk, and L. Hallo, Phys. Rev. B **75**, 195124 (2007).
[26]D. Ivanov and B. Rethfeld, Appl. Surf. Sci. **255**, 9724 (2009).
[27]D. S. Ivanov and L. V. Zhigilei, Phys. Rev. B **68**, 064114 (2003).
[28]D. S. Ivanov, Z. Lin, B. Rethfeld, G. M. OConnor, T. J. Glynn, and L. V. Zhigilei, J. Appl. Phys. **107**, 013519 (2010).
[29]Y. Rosandi and H. M. Urbassek, Appl. Phys. A: Mater. Sci. Process. **101**, 509 (2010).
[30]J. P. Colombier, P. Combis, F. Bonneau, R. Le Harzic, and E. Audouard, Phys. Rev. B **71**, 165406 (2005).
[31]M. E. Povarnitsyn, N. E. Andreev, P. R. Levashov, K. V. Khishchenko, and O. N. Rosmej, Phys. Plasmas **19**, 023110 (2012).
[32]S. I. Anisimov, B. L. Kapeliovich, and T. L. Perel'man, Zh. Eksp. Teor. Fiz. **66**, 776 (1974) [Sov. Phys. JETP **39**, 375 (1974)].
[33]K. Vestentoft and P. Balling, Appl. Phys. A: Mater. Sci. Process. **84**, 207 (2006).
[34]S. I. Anisimov and B. Rethfeld, Proc. SPIE-Int. Soc. Opt. Eng. (USA) **3093**, 192 (1997).
[35]B. N. Chichkov, C. Momma, S. Nolte, F. von Alvensleben, and A. Tünnermann, Appl. Phys. A: Mater. Sci. Process. **63**, 109 (1996).
[36]J. Bonse, A. Rosenfeld, and J. Krüger, J. Appl. Phys. **106**, 104910 (2009).
[37]G. Ferrini, F. Banfi, C. Giannetti, and F. Parmigiani, Nucl. Instrum. Methods Phys. Res., Sect. A **601**, 123 (2009).
[38]E. Carpene, Phys. Rev. B **74**, 024301 (2006).
[39]Z. Lin, L. V. Zhigilei, and V. Celli, Phys. Rev. B **77**, 075133 (2008).
[40]E. Beaurepaire, J.-C. Merle, A. Daunois, and J.-Y. Bigot, Phys. Rev. Lett. **76**, 4250 (1996).
[41]B. Koopmans, G. Malinowski, F. Dalla Longa, D. Steiauf, M. Fähnle, T. Roth, M. Cinchetti, and M. Aeschlimann, Nat. Mater. **9**, 259 (2010).
[42]M. Toulemonde, J. M. Costantini, C. Dufour, A. Meftah, E. Paumier, and F. Studer, Nucl. Instrum. Methods Phys. Res., Sect. B **116**, 37 (1996).
[43]O. Osmani, N. Medvedev, M. Schleberger, and B. Rethfeld, Phys. Rev. B **84**, 214105 (2011).
[44]K. H. Kim, K. Watanabe, D. Mulugeta, H.-J. Freund, and D. Menzel, Phys. Rev. Lett. **107**, 047401 (2011).
[45]L. D. Pietanza, G. Colonna, S. Longo, and M. Capitelli, Eur. Phys. J. D **45**, 369 (2007).
[46]L. Wu and L. K. Ang, Phys. Rev. B **78**, 224112 (2008).
[47]W. Wendelen, B. Y. Mueller, D. Autrique, B. Rethfeld, and A. Bogaerts, J. Appl. Phys. **111**, 113110 (2012).
[48]B. Y. Mueller, T. Roth, M. Cinchetti, M. Aeschlimann, and B. Rethfeld, New J. Phys. **13**, 123010 (2011).
[49]H. Yanagisawa, M. Hengsberger, D. Leuenberger, M. Klöckner, C. Hafner, T. Greber, and J. Osterwalder, Phys. Rev. Lett. **107**, 087601 (2011).
[50]J. Hohlfeld, J. G. Müller, S.-S. Wellershoff, and E. Matthias, Appl. Phys. B: Lasers Opt. **64**, 387 (1997).
[51]D. Steil, S. Alebrand, T. Roth, M. Krauß, T. Kubota, M. Oogane, Y. Ando, H. C. Schneider, M. Aeschlimann, and M. Cinchetti, Phys. Rev. Lett. **105**, 217202 (2010).
[52]V. Recoules, P. Renaudin, J. Clérouin, P. Noiret, and G. Zérah, Phys. Rev. E **66**, 056412 (2002).
[53]B. Rethfeld, Ph.D. thesis, Technische Universität Carolo-Wilhelmina Braunschweig, Germany, 1999.
[54]G. Czycholl, *Theoretische Festkörperphysik*, 3rd ed. (Springer, Berlin, 2008).
[55]E. M. Épshtein, Fiz. Tverd. Tela (Leningrad) **11**, 1787 (1970) [Sov. Phys. Solid State **11**, 2213 (1970)].
[56]N. W. Ashcroft and D. N. Mermin, *Solid State Physics* (Harcourt, New York, 1976).
[57]D. R. Lide, G. Baysinger, L. I. Berger, R. N. Goldberg, H. V. Kehiaian, K. Kuchitsu, G. Rosenblatt, D. L. Roth, and D. Zwillinger, *CRC Handbook of Chemistry and Physics* (CRC Press, Boca Raton, FL, 2005).
[58]R. Binder, H. S. Köhler, M. Bonitz, and N. Kwong, Phys. Rev. B **55**, 5110 (1997).
[59]W.-L. Chan, R. S. Averback, and D. G. Cahill, Appl. Phys. A: Mater. Sci. Process. **97**, 287 (2009).
[60]L. Landau, E. M. Lifshitz, and L. P. Pitaevskii, *Course of Theoretical Physics, Volume 5, Statistical Physics*, 3rd ed. (Pergamon, Moscow, 1980).
[61]H. Petek and S. Ogawa, Prog. Surf. Sci. **56**, 239 (1998).
[62]V. A. Gasparov and R. Huguenin, Adv. Phys. **42**, 393 (1993).
[63]D. Pines and P. Nozières, *The Theory of Quantum Liquids* (Benjamin, New York, 1966).
[64]J. Hohlfeld, Ph.D. thesis, Freie Universität Berlin, 1998.
[65]M. Kaveh and N. Wiser, Adv. Phys. **33**, 257 (1984).
[66]A. H. MacDonald, Phys. Rev. Lett. **44**, 489 (1980).
[67]A. M. Chen, H. F. Xu, Y. F. Jiang, L. Z. Sui, D. J. Ding, H. Liu, and M. X. Jin, Appl. Surf. Sci. **257**, 1678 (2010).
[68]B. H. Christensen, K. Vestentoft, and P. Balling, Appl. Surf. Sci. **253**, 6347 (2007).
[69]N. A. Inogamov and Yu. V. Petrov, Zh. Eksp. Teor. Fiz. **137**, 505 (2010) [J. Exp. Theor. Phys. **110**, 446 (2010)].
[70]B. Cho, K. Engelhorn, A. Correa, T. Ogitsu, C. Weber, H. Lee, J. Feng, P. Ni, Y. Ping, A. Nelson *et al.*, Phys. Rev. Lett. **106**, 167601 (2011).
[71]P. E. Hopkins and P. M. Norris, Appl. Surf. Sci. **253**, 6289 (2007).
[72]Note that the values referring to Refs. 65 and 66 were converted from the electrical resistivity ρ by assuming the Drude model of electrical conduction, resulting in $A = e^2[\rho/T_e^2]n_e/m$.
[73]Note that for phonons the assumption of thermal equilibrium directly at the end of the laser pulse is better justified than for electrons and T_p is rather well defined.